ISSN: 2586-7652 (Print) Vol. 04, No. 02, September 2021
ISSN: 2635-7607 (Online)
International Journal of Advanced Engineering
Source: http://ictaes.org
Manuscript received: July 30, 2021; Revised: August 23, 2021; Accepted: August 25, 2021

FLUKA Simulation Based Study of Cosmic Ray Muon Interactions in Iron as a Prospect for Muon Imaging

Sanjay Sharma Poudel[1], Krishna Bahadur Rai[2] and Rajendra Neupane[1*]

[1]*Department of Physics, Birendra Multiple Campus, Tribhuvan University, Bharatpur, Nepal*
[2]*Department of Physics, Patan Multiple Campus, Tribhuvan University, Lalitpur, Nepal*

neupanerajendra5@gmail.com

Abstract

This work contains to study the muon interactions in the material medium iron based on FLUKA Simulation. The energy deposition by muon and its secondaries in the material was computed. A geometrical design of parallelepiped was implemented and the Gaussian mono-axial beam of muon was propagated in the system consisting of iron. The three primary particles; μ^-, μ^+ and n° were allowed to interact with the hypothetical medium iron. Mean energy, energy escaping the system, number of inelastic interactions, major energy per loss were calculated for each primary particle. The number of secondary particles produced during inelastic collision had also been found out. About 100,000 particles were assumed for interaction. The number of inelastic interactions for μ^+, μ^- and n° when they pass through the iron, was found to be 2619, 1881 and 2425780 respectively. We have investigated the possible way to identify the material based on the energy deposition and the interactions by the muons and its secondaries. This work can be used to investigate the properties of material by counting the incoming and outgoing muon and its secondaries.

Keywords: *Cosmic ray muons, energy deposition, FLUKA Simulation, muon imaging, muon interactions.*

1. Introduction

Corresponding Author : Rajendra Neupane
Author's affiliation : Dept. of Physics, Birendra Multiple Campus, Tribhuvan University, Bharatpur, Nepal
Email: neupanerajendra5@gmail.com
Copyright © ICT-AES

Cosmic rays are high-energy particles with a range of GeV to hundreds of TeV and mostly consisting of protons and atomic nuclei. As the cosmic rays enter the Earth's atmosphere, their collision with atoms and molecules mainly oxygen and nitrogen produces a cascade of hadrons (α-particles, p^+, $\pi^\pm$, $k^\pm$), leptons (μ, e^+, e^-, ν) and radiation (x-rays, γ rays). The interactions in the atmosphere produce high energy muons formed by the decay of pions and kaons through reactions like $\pi^\pm \rightarrow \mu^\pm + \nu_\mu$ and $K^\pm \rightarrow \mu^\pm + \nu_\mu$ respectively. Most of the muons were thought to be created at upper atmosphere and traversed with other particles to earth in conical showers with approximately 1° of the trajectory of the primary particles which created them [1]. High energy muons can even penetrate dense materials like rocks. Cosmic ray muons can also be used for muon imaging similar to X-ray imaging. The benefit of the muons over x-rays is that muons are created naturally from cosmic rays and big machines are not required to perform X-ray imaging. Muons can exist in two forms: μ^- and its antiparticle μ^+. Muons have a rest mass of 105.66 MeV/c^2 [2]. Muon is a highly unstable subatomic particle with a mean life of 2.2 microsecond (μs). Despite a short mean life, due to relativistic time dilation, most high energy muons reach the earth's surface and even beneath the surface. Muons have the decay channels: $\mu^- \rightarrow e^- + \underline{\nu_e} + \nu_\mu$ and $\mu^+ \rightarrow e^+ + \nu_e + \underline{\nu_\mu}$. Mean energy of muons increases the more it travels through materials as low energy muons are removed from the spectrum and only the high energy muons persist. The muon flux at the earth's surface is 1 muon per square centimeter per minute [3]. The mean energy of muons at the production site located at about 9-15 km altitude is 6 GeV which corresponds to the velocity of 0.9998 times the speed of light (c) [4]. The energy distribution is almost flat for energies below 1 GeV and follows $E^{-2.7}$ for energies above 10 GeV.

There has been research on the study of cosmic ray muons as a potential way for imaging of natural and man-made artifacts based on muograpy of different structures using muon scattering including the study of cavities in Chephren's pyramid in Egypt [5], muography of the Pyramid of the Sun at Teotihuacan in Mexico [6] and volcanoes in Mt. Stromboli [7], Puy de Dome [8], Mt. Asama [9].

2. Materials and Methods

FLUKA is a particle physics Monte Carlo simulation package. Many studies related to particle physics can be carried out by using appropriate scoring cards that FLUKA provides by default [10-11]. A successful FLUKA simulation run typically needs at least following information: General Cards, Geometry Description, Materials and Assignment, Physics Settings and Scoring. In this work, linear beams of μ^-, μ^+ and n° were used as the source events for simulations. In each case, a line beam is propagated into the geometry from the top passing through the center of the system. The events are drawn from a Gaussian distribution of cosmic ray muon with mean energy of 4 GeV and full-width-half-maximum (FWHM) 0.471 GeV corresponding to standard deviation of 0.2 GeV. Even though a realistic muon flux was not used in the simulation, a Gaussian muon beam with a mean energy 4 GeV is a good enough approximation. Beam description is incorporated by using BEAM and BEAMPOS cards. Each run consisted of 5 cycles, each with a different random seed and every cycle consisting of 20000 primaries. So, the total events run for each case was 100000. Since FLUKA simulation needs geometry description to run, the constructed geometrical design in this work has three nested parallelepipeds consisting of iron, air, and black hole from center to outward as shown in Figure 1. The system has to be enclosed in a black hole to prevent infinite tracking of the particles where particle trajectories terminate at black hole.

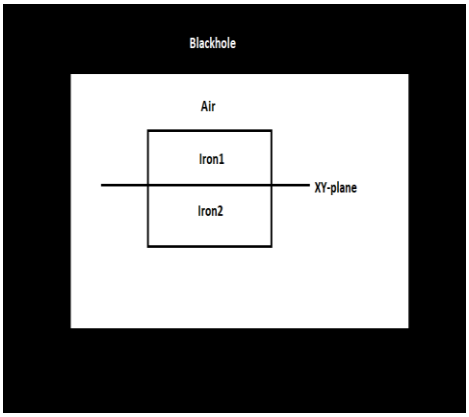


Figure 1. The geometrical structure showing the various regions and materials iron, air, and black hole assigned in the regions.

Figure 1 consists of a nested parallelepiped where black hole forms the outermost structure. The black hole encloses the region of air and it encloses the target region containing an iron target. The region containing the iron target was divided symmetrically by the XY-plane. Different materials assigned in the regions regBH1, Air and Iron1-Iron2 along with the density of the materials assigned to those regions are shown in Table 1.

Table 1. Different materials assigned to different regions and their density.

Region	Material	Density (g/cm^3)
regBH1	Black hole	0
Air	Dry air at NTP	0.00120479
Iron1-Iron2	Iron	7.874

Various physical quantities which we are going to determine in our work can be measured or scored from the simulations. This way Monte Carlo simulations work as a pseudo-detector that can measure desired physical quantities. The common default scoring options used in the simulation were SCORE, USRBDX, USRTRACK, USRBIN. SCORE was used to score inelastic interactions. USRBIN was used to score energy deposition and muon fluence inside and around the target.

Physics models in FLUKA are integrated into the code and each model is bench-marked against the available experimental data. For the simulation study carried out in this work, the default setting was PRECISIO. Most of the physics processes are already activated by using the default as PRECISIO. PHOTONUC card activates photo-nuclear interactions. To activate nucleus-nucleus interactions, 'ldpmqmd' executable was created and linked to the run as prescribed by FLUKA.

3. Results and Discussion

In this section, we have calculated mean energy, full-width-half-maximum (FWHM), energy escaping the system per primary, number of inelastic interactions, major energy loss per primary. These values are obtained when each primary particle: Muon$^-$ (μ^-), Muon$^+$ (μ^+), and Neutron (n°) interact with iron. The number of secondary particles produced during inelastic interaction is also shown.

The important simulation results and outputs are presented in this section.

Table 2. The physics summary for runs involving different particles [Target material: Iron].

Primary particle	Muon$^-$ (μ^-)	Muon$^+$ (μ^+)	Neutron (n°)
Total number of primary	1,00,000	1,00,000	1,00,000
Mean energy, FWHM (GeV)	4, 0.471	4, 0.471	4, 0.471
Energy escaping the system (per primary) (GeV)	1.3492 (32.9%)	1.3475 (32.8%)	0.05498 (1.374%)
Number of inelastic interactions	1881	2619	2425780
Major energy loss per primary	1.8868 (46%)	1.8869 (46%)	1.7069 (43%)
Electromagnetic showers (GeV) per primary	0.859 (20.9%)	0.8603 (21%)	1.4176 (35.4%)
Nuclear recoils and heavy fragments(GeV) per primary	0.0000211 (0.000513%)	0.00002665 (0.00064%)	0.046587 (1.16%)

Table 2 gives an important summary of the simulation runs carried out using different primary beams (muon$^+$, muon$^-$ and neutron) but with same energy distribution. In each case, the material that the primary particle traverses is iron. To generate enough statistics, 100000 primaries were propagated per run. The table shows that energetic muons and neutrons can cause inelastic interactions and produce a lot of secondary particles. Even across 2 meter of iron, we find mean energy deposition is on the order of 2.5 GeV for 4 GeV Gaussian muon mono-axial beams while the remaining energy escapes the system. For the 4 GeV μ^-, μ^+ and n^0, the number of inelastic interactions was obtained to be 1881, 2619 and 2425780 respectively. Relatively, most of energy of μ^-, μ^+ escaped the system corresponding to 32.9% and 32.8% respectively. Typically, energetic muons lose most of the energy in a material by ionization, Bremsstrahlung and hadronic interactions represented as Hadron and muon stopping power (dE/dx) in Table 2. The stopping power (dE/dx) per primary for μ^-, μ^+ and n° is 1.8868 GeV, 1.8869 GeV and 1.7069 GeV respectively. High-energy hadrons are also subjected to inelastic nuclear collisions, which played a major role in the energy dissipation in a material if the hadron energy is of the order of GeV or higher. Energetic neutrons can undergo both elastic and inelastic interactions with material nuclei. Inelastic interactions produce secondary particles like p^+, e^+, e^-, γ that can interact electromagnetically as well. Nuclear collisions are less frequent than Coulomb interactions which is obtained in Table 2. High-energy hadrons still lose some energy in Coulomb interactions before being subjected to a nuclear collision with values of energy deposition per primary about 0.0000211 GeV for μ^-, 0.00002665 GeV for μ^+ and 0.046587 GeV for neutron. The hadrons (protons, neutrons, pions) can form intra-nuclear cascades and the more energetic particles can leave the nucleus. The other particles can deposit their energy in the nucleus and leave the nucleus in an excited state. The table 2 also shows for the same incident energy, there is a much smaller escape of energy from the system for a neutron beam compared to that of a muon beam. The high energy neutrons can be very penetrating and will mainly undergo elastic nuclear collisions until they thermalize and are captured [12]. The table also shows that the features of μ^+ and μ^- are more or less similar. One prominent difference in their interactions is the muon capture on nuclei, which happens for μ^- predominantly.

As the energy of the secondary electron, positron or photon is high enough (> GeV), it gives rise to an electromagnetic shower. The average particle energy decreases from shower generation to shower generation and the cascade development approximately ceases when the energy of electrons and positrons falls below the critical energy, where ionization and excitation processes become dominant. For a 4 GeV μ^-, μ^+ and n°, the energy

loss by production of electromagnetic showers is 0.859 GeV, 0.8603 GeV and 1.4176 GeV respectively. The fraction of energy dissipated by the electromagnetic shower component, increases with the particle energy [13].

Table 3. The number of secondaries generated in inelastic interactions per beam particle type [Target material: Iron].

Primary particle beam type:	μ^-	μ^+	n°
Secondaries produced:			
He^4	342	443	778256
p^+	1392	1831	3187260
γ	2555	3173	521738
n°	2817	3720	6655430
μ^-	351	428	5
π^+	51	82	125738
π^-	52	80	196138
π°	114	160	157688

Table 3 gives the type of the secondaries produced through the muon and neutron interaction in a material iron.

Among the secondaries produced by primary μ^-, 342 He^4, 1392 protons, 2555 gamma rays, 2817 neutrons, 351 muon$^-$ itself, 51 pion$^+$, 52 pion$^-$ and pion$^\circ$ are produced. Relatively more number of secondaries are produced by μ^+ than μ^-. μ^+ produce 443 He^4, 1831 protons, 3173 gamma rays, 3720 neutrons, 82 pion$^+$, 80 pion$^-$ and 160 pion$^\circ$. Due to the relatively low velocity of neutrons, 4 GeV neutrons produce more number of secondaries than muons. Neutrons produce 778256 He^4, 3187260 protons, 521738 gamma rays, 6655430 neutrons, 5 muon$^-$, 125738 pion$^+$, 196138 pion$^-$ and 157688 pion$^\circ$. Neutrons being electrically neutral involves a lot of interactions with the iron target and hence produces a lot of secondaries as shown in Table 3.

The normalized energy deposition (per GeV per primary) for different primary beams for the target material iron is shown in the Fig (2 - 7). The color distribution gives the measure of energy deposition feature in the 2D bins containing iron and the surrounding. Here, black color is associated with maximum energy deposition and white color with minimum or 0 energy deposition.

Figure 2 shows the color distribution of energy deposited per GeV per μ^+ from XY view. The central black color represents the maximum energy deposition in the material corresponding to the energy deposition of 10^{-5} GeV per GeV of muon energy while white color represents no energy deposition at all. Since μ^+ beam has been propagated from the center of the material, it is obvious to have higher energy deposition at the center. Similarly, moving outwards from the center, color becomes lighter representing a lesser amount of energy deposition. The energy deposition seen away from the center is due to the secondary particles produced from the interaction of muons with the material.

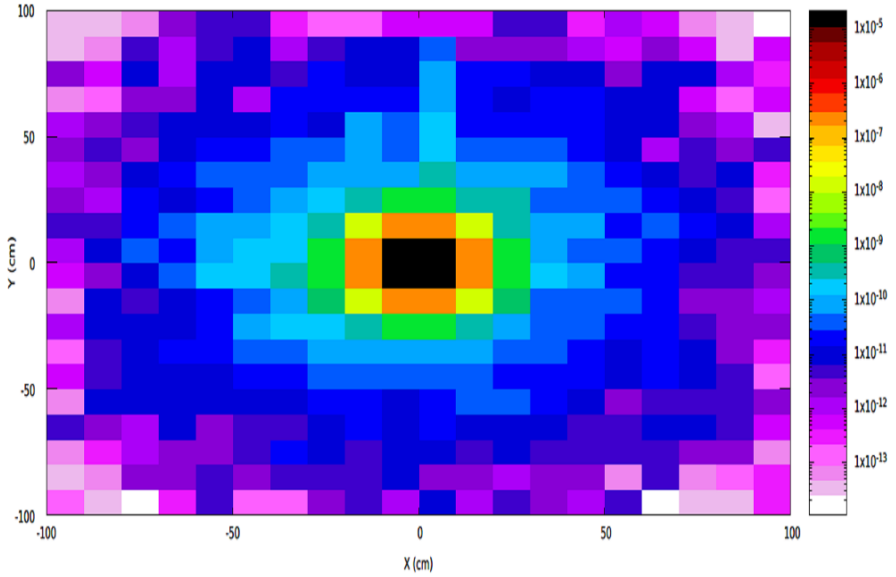


Figure 2. The energy deposition per GeV per muon (XY view) (Beam features: Gaussian μ^+ beam (Mean energy 4 GeV) impinging from the top through [(x, y) = (0,0)], Target: Iron).

Figure 3 shows the color distribution for the energy deposition as viewed from the YZ plane. Since we have propagated μ^+ beam along the Z-axis, black strip at the center can be obtained representing maximum energy deposition along the path of the beam. Some amount of energy can be seen to be deposited even outside the material as a result of the production of hadrons as well as other secondary particles. A distinctive boarder line between the material medium and the air can be obtained which can be exploited to image structures. Even after μ^+ has traversed 200 cm of iron, a significant amount of energy escapes through the material.

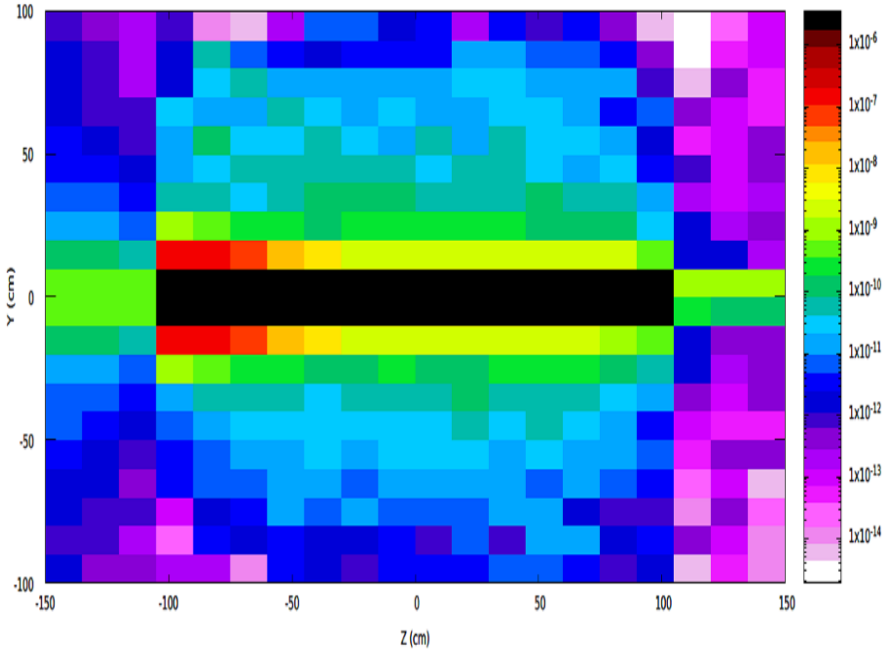


Figure 3. The energy deposition per GeV per muon (YZ view) (Beam features: Gaussian μ^+ beam (Mean energy 4 GeV) impinging from the top through [(x, y) = (0,0)], Target: Iron).

In Figure 4, the energy deposition per GeV per μ^- from XY view is represented. The energy deposition ranges

from 10^{-5} GeV per GeV at the center to 0 at greater distances from the center.

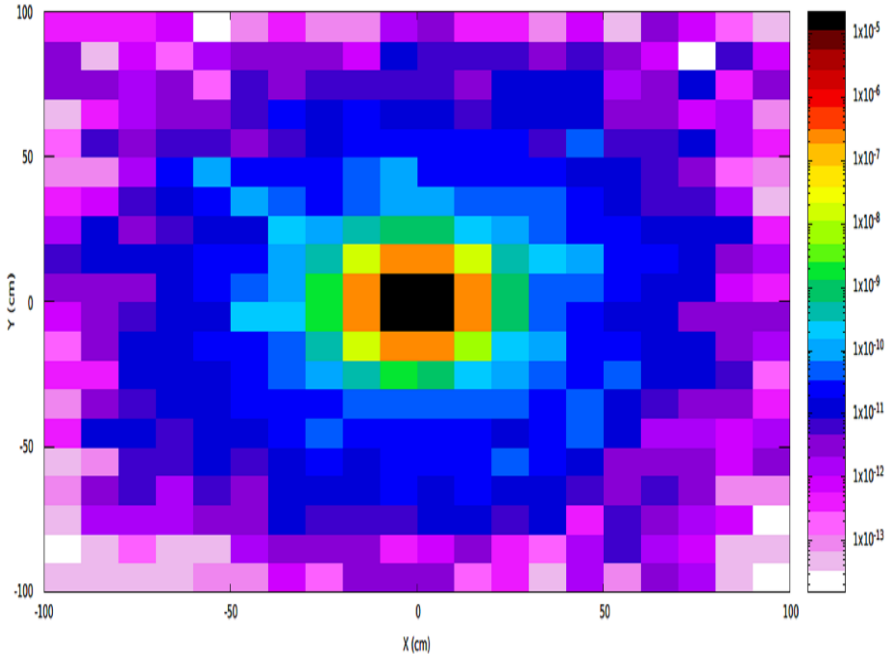


Figure 4. The energy deposition per GeV per muon (XY view) (Beam features: Gaussian μ^- beam (Mean energy 4 GeV). impinging from the top through [(x, y) = (0,0)], Target: Iron)

Figure 5 represents energy deposition per GeV per μ^- along the YZ plane. Similar to figure 3 for μ^+, energy deposition can be seen along the Z-axis where maximum energy is deposited around the center. No significant difference can be seen between the energy deposition by μ^- and μ^+.

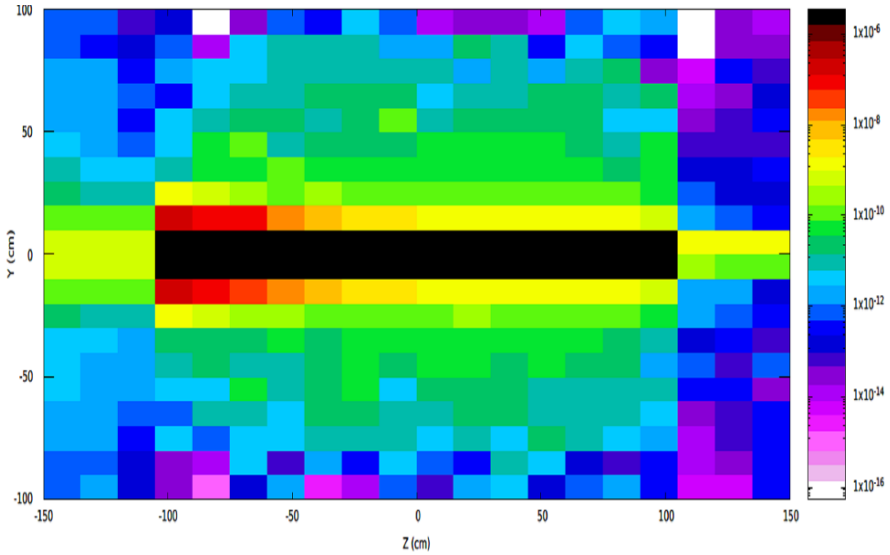


Figure 5. The energy deposition per GeV per muon (YZ view) (Beam features: Gaussian μ^- beam (Mean energy 4 GeV) impinging from the top through [(x, y) = (0, 0)], Target: Iron).

Figure 6 represents the energy deposition per GeV per n° as viewed from the XY plane. Neutron, being a neutral particle involves in a lot of interactions and hence almost all of the energy of neutrons is deposited in the medium. Here, black color corresponds to the maximum energy deposition of 2 x 10^{-5} GeV per GeV of neutron energy and white color represents low or no energy deposition. Similar to μ^- and μ^+, maximum energy is

deposited around the center. The energy distribution for neutrons is more symmetrical than that observed for μ^- and μ^+.

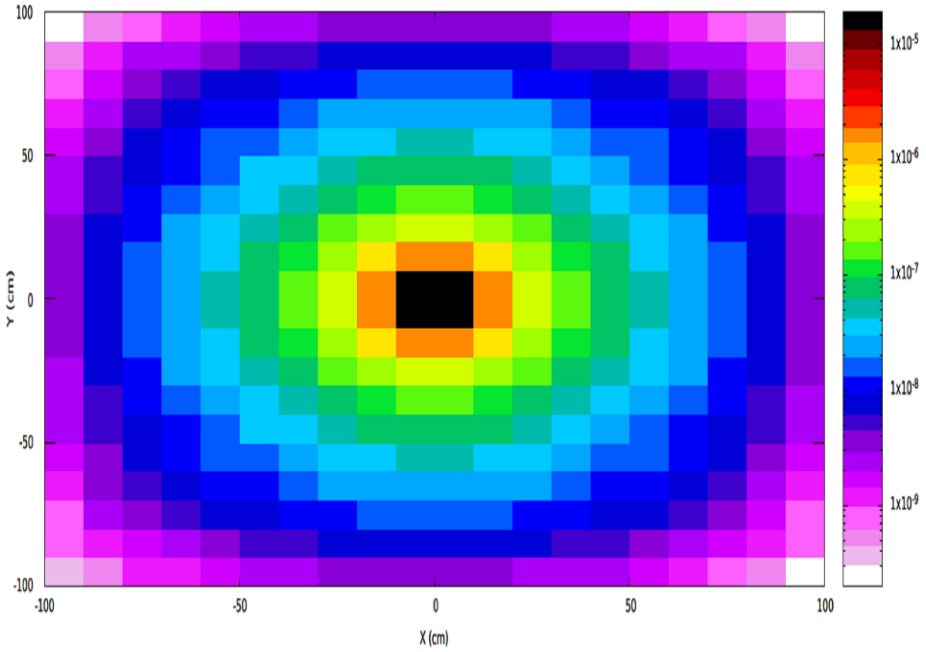


Figure 6. The energy deposition per GeV per neutron (XY view) (Beam features: Gaussian n°beam (Mean energy 4 GeV) impinging from the top through [(x, y) = (0, 0)], Target: Iron).

Figure 7 represents the energy deposition per GeV per neutron along the YZ plane. Neutrons do not have charge and are massive due to which they only traverse a short distance inside the medium iron here. But the secondaries produced by inelastic interaction of neutron and iron travel further and some even out of the material. This shows that a neutron cannot be a good particle for imaging of structures; it loses almost all energy in the interactions and hence does not travel through the medium. Despite seeing a distinct boundary for neutrons, the amount of measurable energy outside the medium is much less and not feasible.

In each of the 2D histograms from Figures (2–7), as expected, most energy is deposited close to the center of iron target material, because the primary beam was directed from the top through (0, 0) in the X-Y plane. While the Gaussian pencil beam may not be a realistic cosmic ray muon beam, the color distribution representing the energy deposition shows that the energy deposition feature in the iron and in the surrounding air is different. Air and iron have different density and composition, and we would expect incoming muons and the resulting secondary particles can have different energy deposition features, which can be exploited with the suitable muon detector medium.

The energy deposition in a material is mediated by Coulomb interactions of charged particles, which are set in motion by atomic and nuclear processes [14]. The ionizing energy loss of a charged particle in a certain volume V can still be different from the energy deposition in V, since the energy can be transported away by δ-rays. Hence, in Figures (2-7) we can observe energy deposited even away from the original beam and as well as the δ-rays.

The distribution of energy deposition is different from μ+, μ- beam compared to that of a neutron beam. The difference is due to the difference in the nature of their interactions as well as their velocities. The energy deposition of the primary muon and the produced secondaries is more localized compared to that of the neutron and its secondaries. The energy deposition in the same material using a muon or neutron beam has different

features. 4 GeV muons are fast as the rest mass of muon is 105.66 MeV/c2 and penetrative, so they penetrate the iron suggesting a good amount of energy of the initial muon primary beam is intact as the muon travels through the iron.

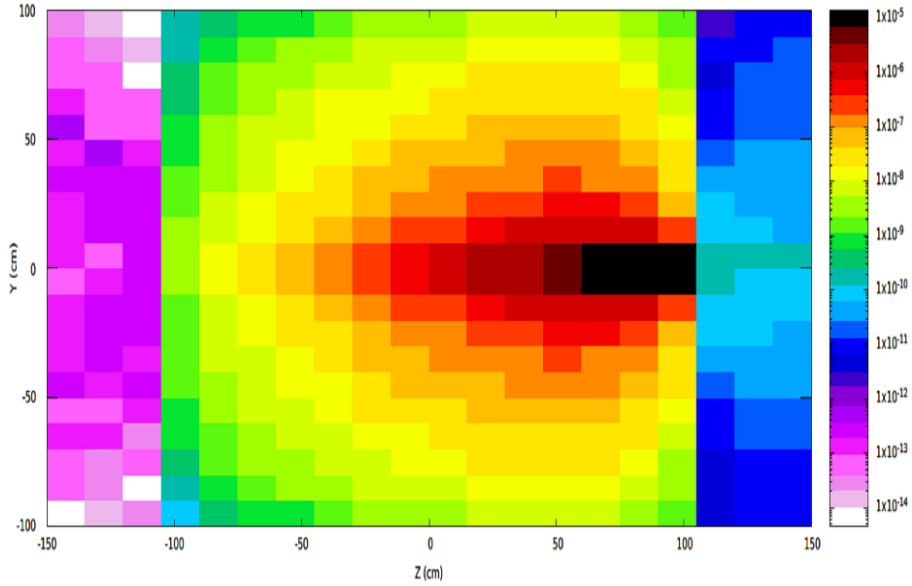


Figure 7. The energy deposition per GeV per neutron (YZ view) (Beam features: Gaussian n° beam (Mean energy 4 GeV) impinging from the top through [(x, y) = (0,0)], Target: Iron).

This is registered as a high percent of escape of the energy of muon primary as it passes through the system. While, a 4 GeV neutron due to its rest mass of ~1 GeV is relatively slow and interacts mostly with the iron nuclei on its way through the material. So, in the case of a neutron beam, the escaping energy is tiny; almost about 1 % which implies that most of the energy of the primary neutron is deposited within the bulk iron in the implemented geometry. Further, it is important to note that the muons, charged and energetic as they are, in our case interact with the material and lose energy mostly by ionization of the material medium and Bremsstrahlung. These interactions can produce other secondaries like e^+, e^-, γ that can interact within the material itself. While the neutron, electrically neutral particle mostly scatters off target nuclei and not the atomic electrons. But in the energetic collisions as in this case, the resulting neutron interactions can produce secondaries off the atom or nuclei. The energetic collisions like the one simulated in our case also shows that there are a lot of inelastic interactions and hence a lot of secondary particles are produced per primary as tabulated in Table.3.

For same geometry and beam characteristics, the normalized energy deposition as a function of thickness Z in cm of iron are shown in Figure 8 for muon$^-$ and in Figure 9 for muon$^+$.

Figure 8 shows histogram for the energy deposition per GeV per μ^- along the Z-axis. For material medium iron, from -100 to 100 cm along the Z-axis we can see a considerable amount of energy deposited in the medium which has been normalized to per GeV per muon. A slight slant in Figure 8 from -100 to 100cm is due to the slowing down of the muons as it traverses the medium owing to electronic and nuclear collisions which results in lesser amount of energy per GeV of muon being deposited onto the material iron.

Figure 9 represents the histogram for energy deposition per GeV per μ+ along the axis of propagation, Z-axis. Similar to Figure 8 for μ-, energy deposition is minimal in air and more in iron medium. The energy deposition ranges from 0 to 5.5 x 10^{-7} GeV per GeV of muon energy. The total energy deposition can be computed by multiplying the obtained energy deposition by the initial energy of muons and number of muons propagated.

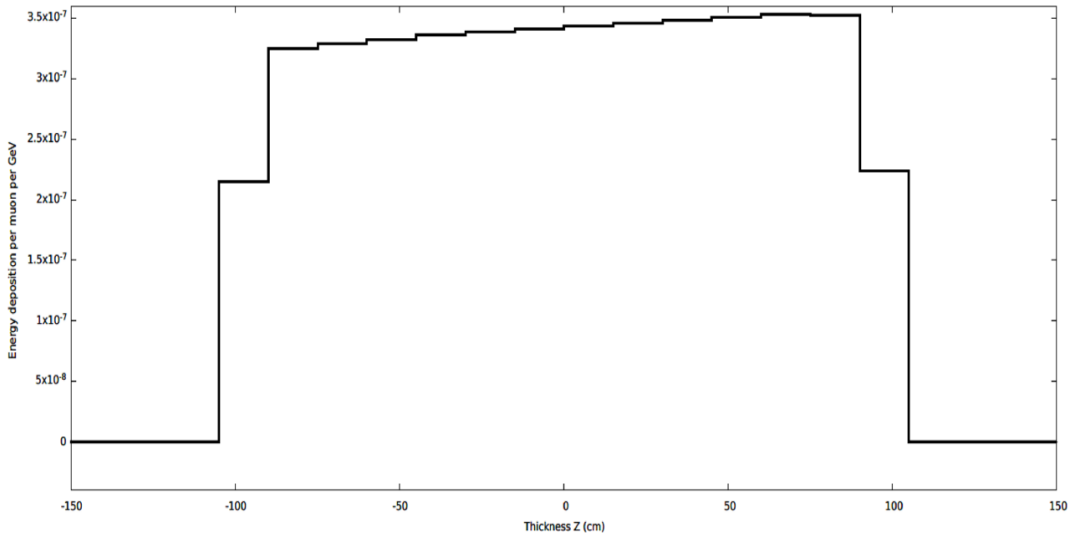


Figure 8. The histogram representing energy deposition per GeV per muon (Z axis) (Beam features: Gaussian μ^- beam (Mean energy 4 GeV) impinging from the top through [(x, y) = (0, 0)], Target: Iron).

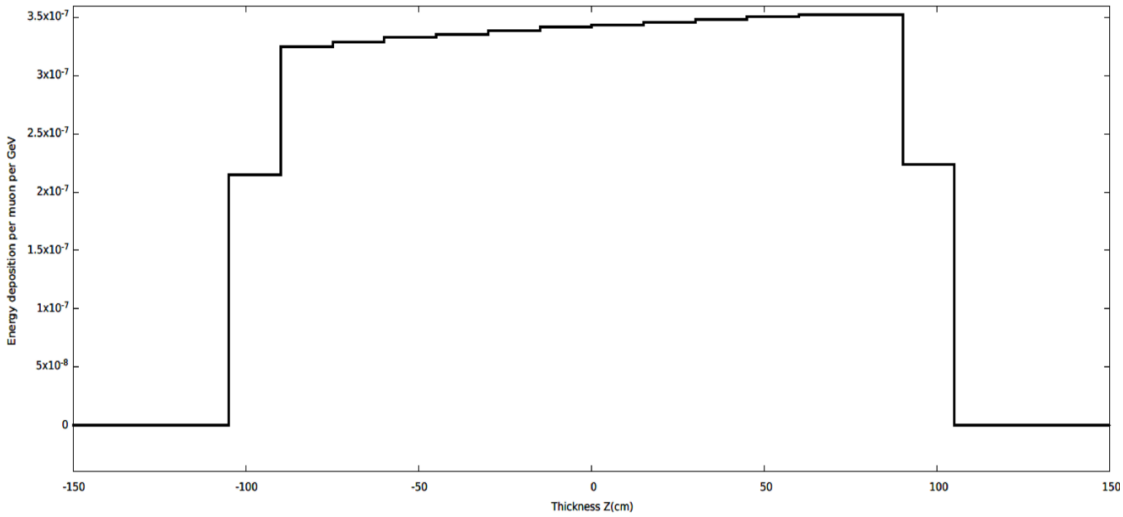


Figure 9. The histogram representing energy deposition per GeV per muon (Z axis) (Beam features: Gaussian μ^+ beam (Mean energy 4 GeV) impinging from the top through [(x, y) = (0, 0)], Target: Iron)

4. Conclusion

On passing through 2 meters of iron, the energetic muon retains energy greater than 30% compared to that by the same energy neutron which is on the order of about 1.5%. This simulation-based study shows that there are certain features of muon interactions that can be exploited to draw some conclusion about the material muon passes through. This study also shows that the energetic muon$^-$ induced interactions produce a lot of secondary particles including photons and electrons, which in principle can be detected and possibly be used to extract the information about the material. While the flux (approximately 1 per cm^2 per minute) is not so high compared to the one produced in the colliders, a long enough total simulation lifetime can provide a means of studying and investigating the features of materials similar to X-ray imaging. The muon interacting in the material can leave enough detectable energy and also pass through several meters of common materials. This makes a cosmic ray muon detector system (possibly a pair of detectors across the material under investigation) an exciting prospect. Such a detector system could detect and measure the counts and the energies of the incoming and outgoing cosmic ray muons or its secondaries allowing us to study the structure or the properties of the material. Some

possible applications of muon-imaging could be locating the underground cavern, investigating non-interferingly the structure of materials in old buildings and temples, studying the fissures in earth's crust etc.

Acknowledgement

We would like to extend our deep gratitude to Dr. Sagar Sharma Poudel for his assistance.

References

1. Borozdin, K. N., Hogan, G. E., Morris, C., Priedhorsky, W. C., Saunders, A., Schultz, L. J. and Teasdale, M. E. 2015. Radiographic imaging with cosmic-ray muons. *Nature*, **422(**6929), 277-277.
2. Mohr, P. J., Newell, D. B., Taylor, B. N. and Tiesinga, E. 2019. The NIST Reference on Constants, Units, and Uncertainty.
3. Griffiths, D. 2020. *Introduction to elementary particles*. John Wiley and Sons.
4. Hayakawa, S. 1969. Cosmic ray physics. Nuclear and astrophysical aspects. *Interscienc**e** Monographs and Texts in Physics and Astronomy.*
5. Alvarez, L. W., Anderson, J. A., El Bedwei, F., Burkhard, J., Fakhry, A., Girgis, A., and Yazolino, L. 1970. Search for hidden chambers in the pyramids. *Science*, **167**(3919), 832-839.
6. Aguilar, S., Alfaro, R., Belmont, E., Grabski, V., Ibarra, T., Lemus, V., ... & Sandoval, A. 2013. Search for cavities in the Teotihuacan Pyramid of the Sun using cosmic muons: preliminary results. In *International Cosmic Ray Conference*, **33**, 2003.
7. Tioukov, V., Alexandrov, A., Bozza, C., Consiglio, L., D'Ambrosio, N., De Lellis, G., ... & Tanaka, H. K. (2019). First muography of Stromboli volcano. *Scientific reports*, **9**(1), 1-11.
8. Ambrosino, F., Anastasio, A., Bross, A., Béné, S., Boivin, P., Bonechi, L., and Vulpescu, B. (2015). Joint measurement of the atmospheric muon flux through the Puy de Dôme volcano with plastic scintillators and Resistive Plate Chambers detectors. *Journal of Geophysical Research: Solid Earth*, **120**(11), 7290-7307.
9. Tanaka, H. K., Nakano, T., Takahashi, S., Yoshida, J., Takeo, M., Oikawa, J., ... & Niwa, K. (2007). High resolution imaging in the inhomogeneous crust with cosmic-ray muon radiography: The density structure below the volcanic crater floor of Mt. Asama, Japan. *Earth and Planetary Science Letters*, **263**(1-2),104-113.
10. Fasso, A., Ferrari, A., Ranft, J. and Sala, P. R. 1995. An update about FLUKA. *In Proc. 2nd workshop on Simulating Accelerator Radiation Environment, SARE-2,* CERN-Geneva, 9.
11. Fasso, A., Ferrari, A., Ranft, J. and Sala, P. R. 2005. FLUKA: *a multi-particle transport code*, **1**, 24 - 28. CERN.
12. Scheck, F. (1978). Muon physics. *Physics Reports*, **44**(4), 187-248.
13. Sato, T., Niita, K., Matsuda, N., Hashimoto, S., Iwamoto, Y., Noda, S. and Sihver, L. (2013). Particle and heavy ion transport code system, PHITS, version 2.52. *Journal of Nuclear Science and Technology*, **50**(9), 913-923.
14. Gorringe, T. P., & Hertzog, D. W. (2015). Precision muon physics. *Progress in Particle and Nuclear Physics*, **84**, 73-123.